Gluing bifurcations in Chua oscillator

Article *in* International Journal of Bifurcation and Chaos · December 2006

DOI: 10.1142/S021812740601694X · Source: DBLP

CITATIONS
11

READS
157

2 authors:

Prodyot Kumar Roy
Presidency University, Kolkata
63 PUBLICATIONS **708** CITATIONS
SEE PROFILE

Syamal Kumar Dana
Jadavpur University
142 PUBLICATIONS **2,294** CITATIONS
SEE PROFILE

International Journal of Bifurcation and Chaos, Vol. 16, No. 12 (2006) 3497–3508

GLUING BIFURCATIONS IN CHUA OSCILLATOR

PRODYOT KUMAR ROY
Department of Physics, Presidency College,
Kolkata 700 073, India
pkpresi@yahoo.co.in

SYAMAL KUMAR DANA
Instrument Division,
Indian Institute of Chemical Biology,
Kolkata 700 032, India
skdana@iicb.res.in

Received August 24, 2005; Revised October 25, 2005

Gluing bifurcation in a modified Chua's oscillator is reported. Keeping other parameters fixed when a control parameter is varied in the modified oscillator model, two symmetric homoclinic orbits to saddle focus at origin, which are mirror images of each other, are glued together for a particular value of the control parameter. In experiments, two asymmetric limit cycles are homoclinic to the saddle focus origin for different values of the control parameter. However, imperfect gluing bifurcation has been observed, in experiments, when one stable and unstable limit cycles merge to the saddle focus origin via saddle-node bifurcation.

Keywords: Chua oscillator; homoclinic bifurcation; gluing bifurcation.

1. Introduction

Gluing bifurcation in reflection symmetric systems is an important class of homoclinic bifurcation where two periodic orbits become homoclinic to a saddle type limit set. The trajectory of a homoclinic orbit tends [Wiggins, 1990] to a saddle for both forward and backward in time. In the neighborhood of this homoclinic orbit, the period of the limit cycle increases asymptotically or in a wiggle [Glendinning & Sparrow, 1984; Gaspard *et al.*, 1984] to infinity with a control parameter since the trajectory spends longer and longer time as it moves closer to the saddle. In case of gluing bifurcation, a limit cycle approaches homoclinicity, moreover, another coexisting limit cycle becomes homoclinic to the saddle for the same value of the control parameter. At the bifurcation point two homoclinic orbits, which are mirror images of each other, appear as glued together at the saddle and form a periodic orbit with a figure of shape eight [Wiggins, 1990].

Gluing bifurcation has already been observed experimentally in a few reflection symmetric systems. Experiments include liquid crystal flow [Peacock & Mullin, 2001], Taylor–Couette flow [Marques *et al.*, 2002], optothermal nonlinear device [Herrero *et al.*, 1998], and electronic van der Pol oscillator [Glendinning *et al.*, 2001]. This is also reported in numerical investigations of Lorenz system [Pazo & Perez-Munuzuri, 2002]. It is interesting to note that the signatures of gluing bifurcation have also been found in nature as reported recently in human heart rate variability [Zebrowski & Baranowski, 2003] of several patients with increased arrhythmia.

In experimental systems, perfect reflection symmetry is never achievable due to several sources of natural imperfections including the presence of

noise both internal and external. In such asymmetric systems, imperfect gluing bifurcation can only be observed when two asymmetric periodic orbits are homoclinic to a saddle point for different values of the control parameter. With change in a control parameter, one limit cycle attains homoclinicity and then merges with a saddle cycle via saddle-node (SN) bifurcation. Finally, by an exchange of stability, the saddle cycle becomes stable and then homoclinic to the saddle for a different value of the control parameter.

In this paper, we report our observations on gluing bifurcation in electronic Chua oscillator via numerical simulation as well as experiment. For this, the original circuit is slightly modified in order to restrict the dynamics to single scroll limit cycle only, however, keeping the properties of reflection symmetry undisturbed. The bistability of the circuit is also unaffected by this modification. Bistability is an important criterion for gluing bifurcation in reflection symmetric systems.

The paper is organized as follows: the electronic circuit, its model equations, and bifurcation properties are described in the next section. Results of numerical simulations on gluing phenomenon and related period-parameter bifurcation are elaborated in Sec. 3 while the experimental results are presented in Sec. 4 with a brief conclusion in Sec. 5.

2. The Modified Chua Oscillator

The modified Chua circuit is shown in Fig. 1, which contains one variable resistor (R_1), two capacitors (C_1 and C_2) and one inductor (L) with a leakage resistance (r_0) and, a nonlinear resistance approximated by two op-amps (U1-U2:μA741) and associated linear resistances. The values of various circuit components used for both experiment and numerical simulations are noted in the circuit diagram. Adding another variable resistor (R_p) parallel to the nonlinear resistor makes a little modification in the original circuit, which enables smooth control over its complex dynamics. The modified model is given by

$$\frac{dV_{C_1}}{dt} = \frac{G}{C_1}\left[V_{C_2} - \left(1 + \frac{R_1}{R_p}\right)V_{C_1}\right] - \frac{1}{C_1}f(V_{C_1}) \tag{1a}$$

$$\frac{dV_{C_2}}{dt} = \frac{1}{C_2}[I_L - G(V_{C_2} - V_{C_1})] \tag{1b}$$

$$\frac{dI_L}{dt} = -\frac{1}{L}(V_{C_2} + r_0 I_L) \tag{1c}$$

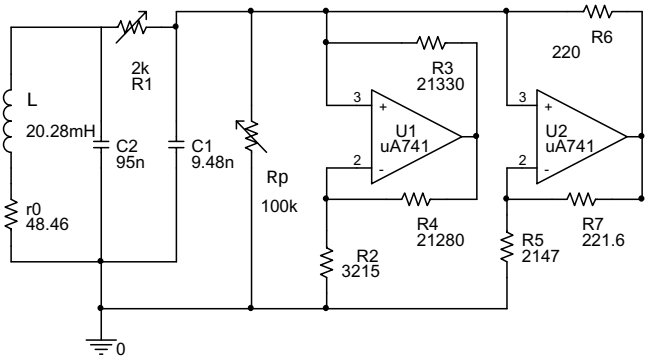

Fig. 1. Modified Chua Circuit: All component values noted below each component, except R_1 and R_p, which are variable. Power supply is ± 9 V.

where the piecewise linear function $f(V_{C1})$ is given by

$$f(V_{C_1}) = \begin{cases} G_b V_{C_1} + (G_b - G_a)E & \text{if } V_{C_1} < -E \\ G_a V_{C_1} & \text{if } -E \le V_{C1} \le E \\ G_b V_{C_1} + (G_a - G_b)E & \text{if } V_{C1} > E \end{cases} \tag{1d}$$

and the slopes G_a and G_b are

$$G_a = \left(-\frac{1}{R_2} - \frac{1}{R_4}\right), \quad G_b = \left(\frac{1}{R_3} - \frac{1}{R_4}\right) \tag{2}$$

The state variables are the voltages V_{C1} and V_{C2} across the capacitors C_1 and C_2 respectively and the inductor current I_L through the inductor L. $G = 1/R_1$, and the op-amp saturation voltage is $E \approx 1$. The first equation is only changed by the modification in the original circuit, which is restored for large R_p values. The system has three equilibrium points: one inner saddle focus at the origin and the other two outer saddle foci at mirror symmetric positions [Chua *et al.*, 1986; Dana *et al.*, 2004]. The eigenvalues of the saddle focus origin are $(\gamma, -\sigma \pm j\omega)$, while they are $(-\gamma, \sigma \pm j\omega)$ for both the mirror symmetric saddle foci.

When the value of the resistor R_p is large enough to allow almost no current through it, the circuit behaves like the original Chua circuit. In such a situation if R_1 is reduced from large values, keeping all other parameters fixed at the selected values, the circuit dynamics undergoes successive bifurcations [Chua *et al.*, 1986]: super-Hopf, period doubling (PD) leading to chaos, followed by intermediate periodic windows via period-adding and PD again leading to chaos. With further reduction in R_1, transition to double scroll chaos is observed followed by period-adding bifurcation, reverse PD

to period-1 orbit and then sub-Hopf. In contrast, if we set a suitably small value of R_p, the dynamics may fully be restricted to single scroll period-1 limit cycle only. This limit cycle appears via super-Hopf and grows in amplitude with reduction in R_1 and then undergoes sub-Hopf forming an unstable limit cycle. If R_p is then made slightly larger, by gradually decreasing R_1, we can observe period-1 and period-2 limit cycles via super-Hopf and PD and then reverse PD followed by sub-Hopf. For even larger and larger values of R_p, higher periodic orbits like period-4 or period-8 and so on starts appearing thereby leading to original Chua circuit dynamics.

A typical bifurcation diagram for a selected $R_p = 10.375\,\mathrm{k}\Omega$ is obtained from numerical simulation as shown in Fig. 2 by plotting the $\max(V_{C1}(\mathrm{t}))$ with R_1. A back-to-back Hopf bifurcation with intermediate PD to period-2 limit cycle (in red dots) and then reverse PD are seen. The bistability property is evident from two separate back-to-back bifurcation plots corresponding to maxima of coexisting limit cycles. In another bifurcation diagram for $R_p = 10.8\,\mathrm{k}\Omega$ shown in Fig. 3 back-to-back Hopf is still observed but with intermediate period-4 limit cycles (blue trace) and also orbits of higher periodicity. First a period-1 limit cycle appears via super-Hopf (red trace) followed by period-2 (green trace) and period-4 (blue trace) via successive PD at $R_1 = 1563\,\Omega$ and $R_1 = 1517\,\Omega$, respectively. The period-2 cycle reappears (green trace) via reverse PD for $R_1 = 1502\,\Omega$. The period-2 gluing orbit is observed at $R_1 = 1495\,\Omega$ near the kink during the change over from green to yellow trace. The yellow trace actually indicates the big period-2 limit cycle after the gluing. A narrow region in magenta trace follows close to $R_1 = 1471\,\Omega$, which includes orbits of higher periodicity even larger than period-4. The period-4 limit cycle (blue) reappears at $R_1 = 1470\,\Omega$ via PD, which undergoes reverse PD again for twice at $R_1 = 1468\,\Omega$ and $R_1 = 1462\,\Omega$ respectively to reach finally to a period-1 limit cycle.

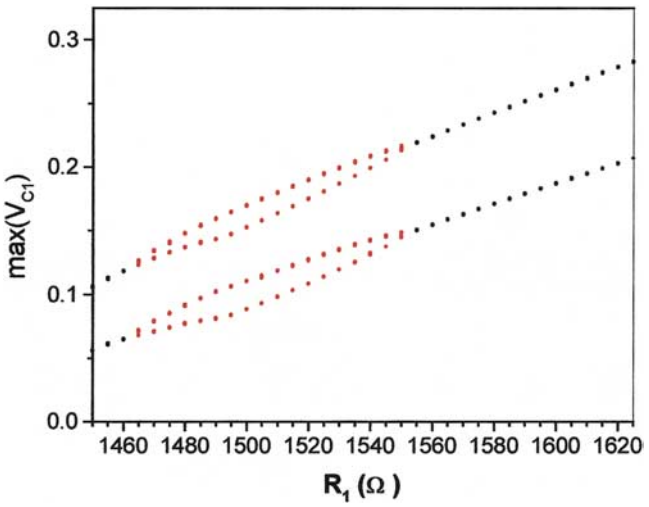

Fig. 2. Back to back Hopf bifurcation diagram at $R_p = 10.375\,\mathrm{k}\Omega$.

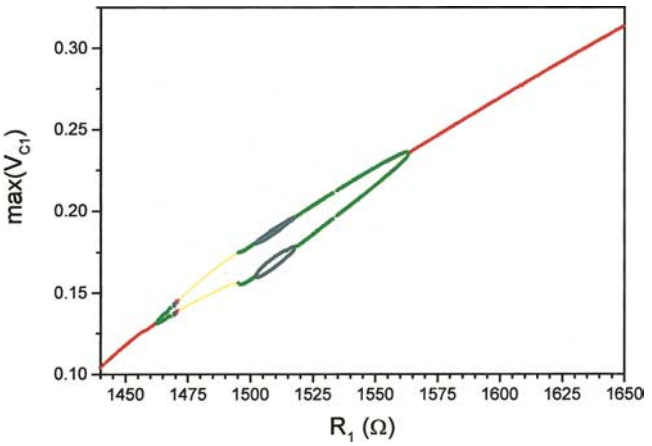

Fig. 3. Back to back Hopf bifurcation diagram at $R_p = 10.8\,\mathrm{k}\Omega$.

3. Gluing Bifurcation

For observing gluing bifurcation in numerical simulations we proceed as follows: select a suitable value of R_p and then vary R_1 keeping all other parameters fixed. First, we set $R_p = 10.5\,\mathrm{k}\Omega$ which restricts the dynamics to period-2 oscillations only. Then as we reduce R_1 from high value, a period-1 limit cycle first appears via super-Hopf around one of the outer equilibrium points and subsequently becomes period-2 via PD. With further decrease in R_1, the period-2 limit cycle tends to the saddle focus origin when the trajectory spirals into and escapes away from a close neighborhood of the saddle focus at $R_1 = 1488.73\,\Omega$. This periodic orbit is labeled as 0^2 in Fig. 4(a), which is obtained for R_1 very close to the value corresponding to a homoclinic orbit. The superscript denotes periodicity of the limit cycle. There coexist another period-2 orbit, which is a mirror image of the former labeled by 1^2 and shown in Fig. 4(b). This pair of period-2 orbits finally merges at the bifurcation point to form a symmetric orbit around the origin. In phase space it appears as two mirror symmetric period-2 homoclinic orbits as if glued together at the origin (inner saddle

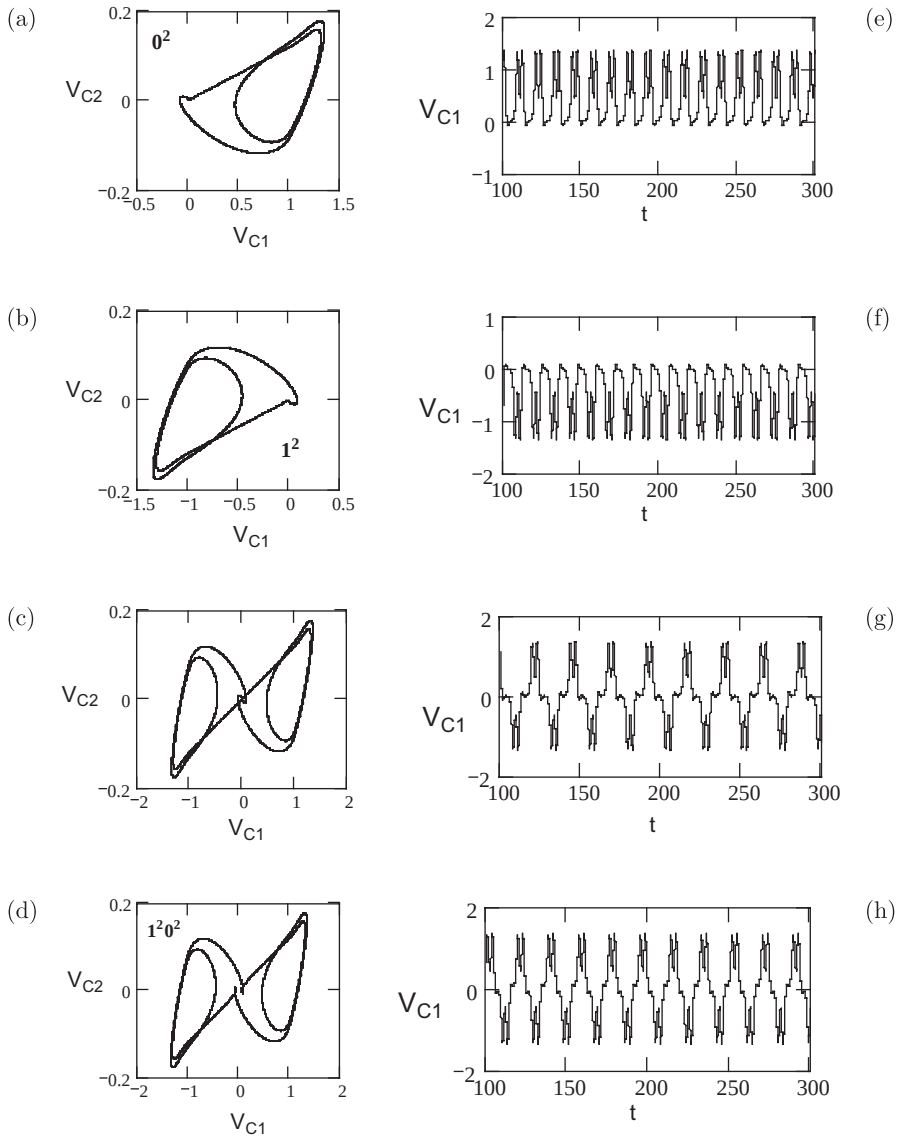

Fig. 4. Numerical gluing bifurcation: phase portraits of a sequence of bifurcation leading to periodic orbits 0^2, 1^2 for $R_1 = 1488.73\,\Omega$, gluing orbit for $R_1 = 1488.72\,\Omega$, and a big orbit $1^2 0^2$ for $R_1 = 1488.65\,\Omega$ as shown in the left column from (a)–(d) rows, respectively. The corresponding time series are shown in (e)–(h) next to each of them in the right column, $R_p = 10.5\,\mathrm{k}\Omega$.

focus) as shown in Fig. 4(c) for $R_1 = 1488.72\,\Omega$. For further decrease in R_1 the glued orbit breaks into a large period-2 orbit (labeled by $1^2 0^2$) shown in Fig. 4(d) for $R_1 = 1488.65\,\Omega$. The corresponding time series for 1^2, 0^2, gluing orbit and $1^2 0^2$ are shown in Figs. 4(e)–4(h) in the right column.

The period-parameter bifurcation (T versus R_1) is shown in Fig. 5. The dynamics first undergoes super-Hopf and then PD during transition from the red to green trace on the right with decrease in R_1. The time period plots corresponding to 0^2 and 1^2 limit cycles cannot be separated since their periods remain always identical in symmetric system. The period of both the limit cycles 0^2 and 1^2 increases asymptotically with reduction in R_1 and become homoclinic to the saddle focus origin for $R_1 = 1488.73\,\Omega$. This homoclinic point corresponds to the first peak (green line) from the right side in the period-parameter space when two mirror symmetric period-2 limit cycles (0^2 and 1^2) glued together as shown in Fig. 4(c) at $R_1 = 1488.72\,\Omega$. Beyond this first peak, the period shows a discontinuity on the left side, when the periodic orbits

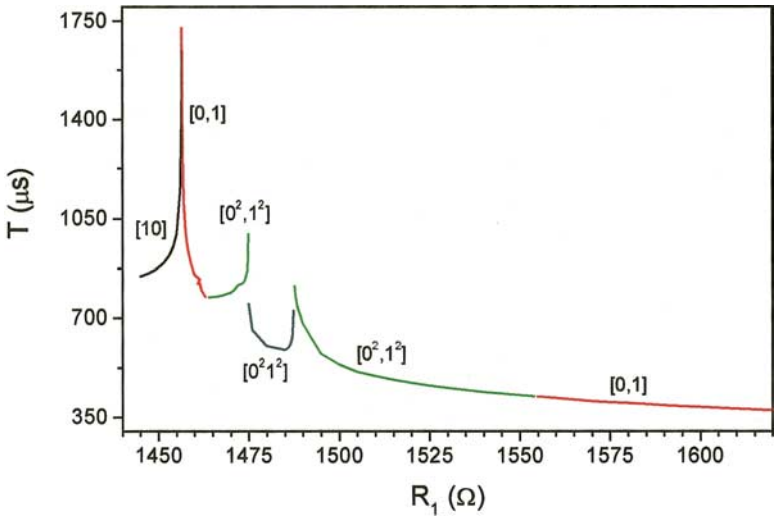

Fig. 5. Period parameter ($T - R_1$) bifurcation diagram ($R_p = 10.5\,\mathrm{k}\Omega$).

(0^2 and 1^2) switch over to another periodic orbit (1^20^2). The period of 1^20^2 orbit then starts decreasing (blue trace) with decrease in R_1 but starts increasing asymptotically again after passing through an intermediate minimum. The 1^20^2 orbit then switches to another periodic orbit at a second gluing point as indicated by a second peak (green line) in Fig. 5 at $R_1 = 1474.9\,\Omega$. For $R_1 < 1474.9\,\Omega$, the time period decreases again when a reverse PD to period-1 orbit is observed. We find a third peak from the right (red line) at $R_1 = 1454.857\,\Omega$, which corresponds to period-1 homoclinic orbit labeled by 0 as shown in Fig. 6(a). There coexists another orbit labeled by 1 shown in Fig. 6(b). The mirror symmetric $(0, 1)$ orbits then glued together at the saddle focus origin for $R_1 = 1454.827\,\Omega$ as shown in Fig. 6(c). The gluing orbit finally breaks again into a large period-1 orbit (labeled by 10) at $R_1 = 1488.6\,\Omega$ in Fig. 6(d). The period of this large period-1 orbit decreases monotonically as indicated by the black line and become unstable via sub-Hopf. The corresponding time series are shown in Figs. 6(e)–6(h). It may be noted that the period-parameter curves, in reality, are disconnected lines corresponding to different periodic orbits. The intermediate discontinuities between continuous lines indicate regions of irregularity during each transition of periodic orbit of one type to another. The irregular regions in parameter space as observed in numerical simulations are, however, very narrow. They are more prominent in experiments as described in the next section.

Next we tried with a higher $R_p = 10.8\,\mathrm{k}\Omega$ when we also observed back-to-back Hopf with successive PD to period-4 orbit followed by reverse PD for twice to period-1 and then sub-Hopf. The corresponding period-parameter bifurcation in Fig. 7 shows five peaks indicating five gluing points. Thus for increase in R_p value, more and more gluing points arise, which correspond to higher order periodic orbits. This is illustrated in a two-parameter ($R_p - R_1$) bifurcation in Fig. 8 that shows different periodic regimes in colors separating the bifurcation boundaries. The boundary between black and red regions at the top indicates the super-Hopf so that the red region belongs to period-1 limit cycle. The green region belongs to period-2 and hence the border of red and green indicates either forward PD at the upper side or reverse PD at the lower side. Similarly, the blue region is for period-4 limit cycle, whose periphery indicates forward or reverse PD at the top or bottom, respectively. The boundary of the yellow region demarcated by black dots is the locus of gluing bifurcation inside which a large periodic orbit labeled by 1^20^2 exists. On this bifurcation locus, two period-2 orbits are homoclinic to the saddle focus at the origin. The boundary of green and red regions at the bottom for $R_p < 10.425\,\mathrm{k}\Omega$ indicates the locus of another gluing bifurcation when two period-1 orbits are homoclinic to the saddle focus at origin. The bottom red region belongs to large periodic orbit labeled by 10. Gluing of two period-1 orbits can be observed at the crossing of red to green from the bottom for $R_p < 10.425\,\mathrm{k}\Omega$

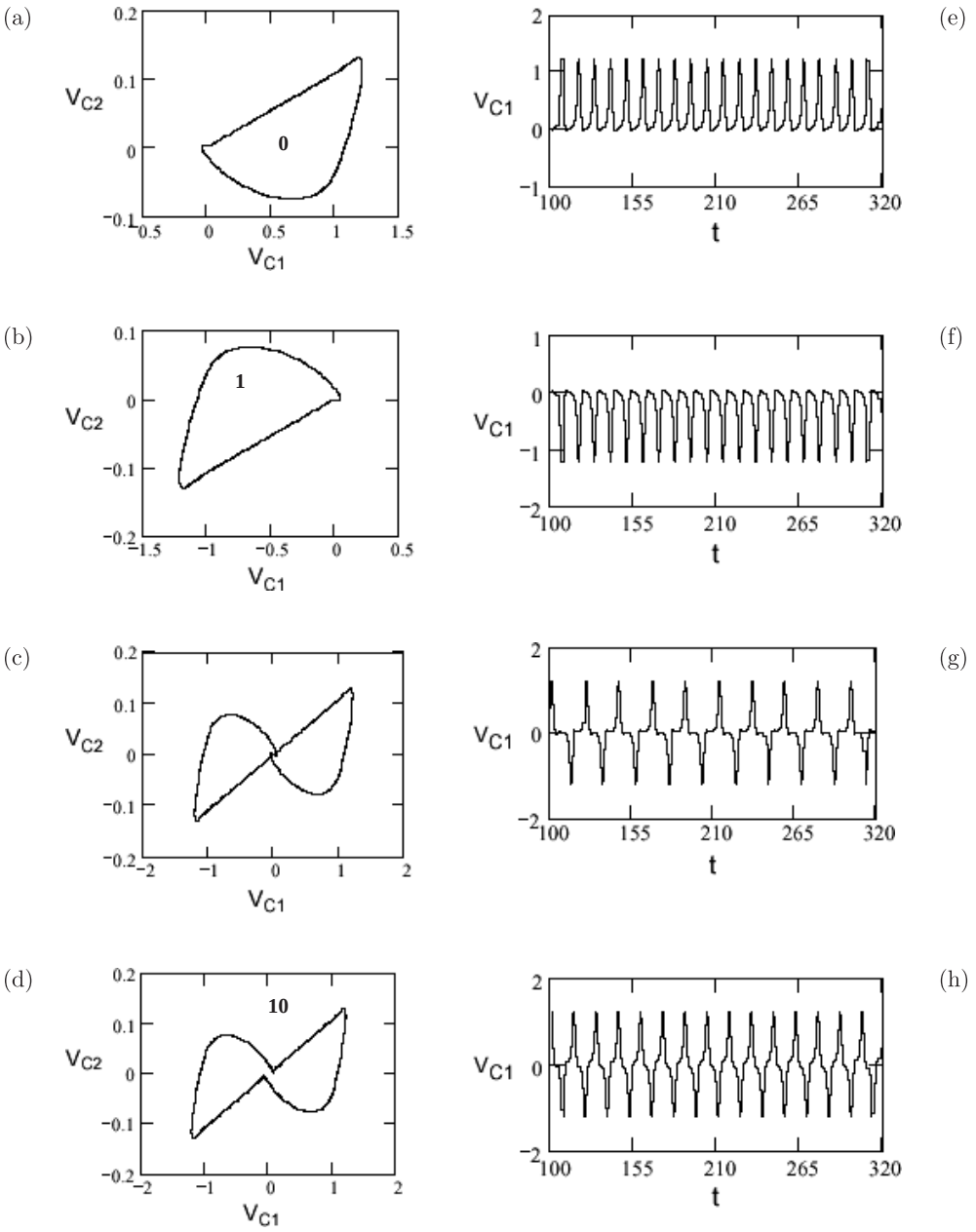

Fig. 6. Numerical gluing bifurcation: phase portraits of a sequence of bifurcation leading to periodic orbits $[0, 1]$ for $R_1 = 1454.857\,\Omega$, gluing orbit for $R_1 = 1454.827\,\Omega$, and a big 10 orbit for $R_1 = 1454.6\,\Omega$ as shown in the left column from top to bottom, respectively. The corresponding time series are shown next to each of them in the right column. $R_p = 10.5\,\mathrm{k}\Omega$.

only. For $R_p > 10.425\,\mathrm{k}\Omega$ i.e. on the right of the folding point F (with $R_p = 10.425\,\mathrm{k}\Omega$, $R_1 = 1481\,\Omega$) of the black dotted boundary of the yellow region, gluing of 1^2 and 0^2 orbits can be observed in addition to gluing of period-1 orbits. In contrast, when R_p is larger ($>10.7\,\mathrm{k}\Omega$), more complicated dynamics appear and more and more gluing points of higher periodic orbits starts appearing. This is indicated by a few scattered points in magenta near the border of yellow and green. This ultimately leads to chaos when R_p becomes very large. The increasing number of gluing points with increasing R_p becomes really difficult to resolve because of their narrow regions of separation in parameter space. Presently, we restricted our study on a range of $R_p = 10.375\,\mathrm{k}\Omega$ to $11\,\mathrm{k}\Omega$ to have a fair idea of the most simple examples of gluing orbits that can be observed in the dynamics of Chua oscillator.

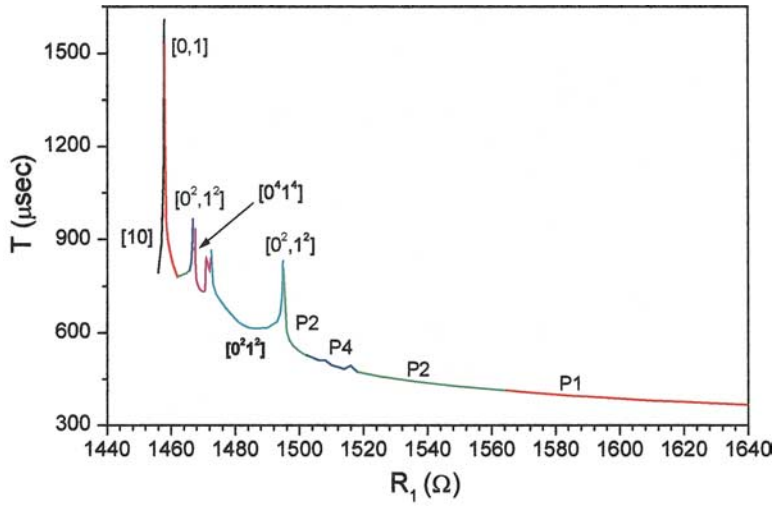

Fig. 7. Period parameter bifurcation diagram ($R_p = 10.8\,\mathrm{k}\Omega$).

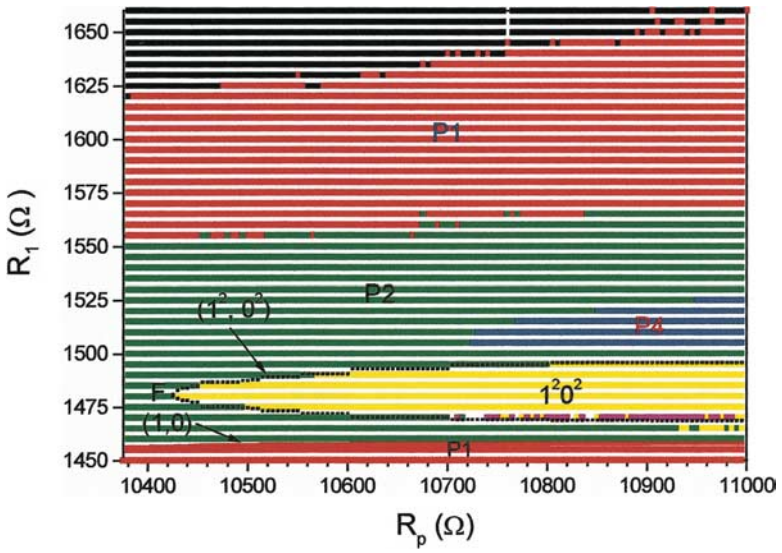

Fig. 8. Two parameter ($R_p - R_1$) bifurcation diagram.

4. Experiment: Imperfect Gluing Bifurcation

We already mentioned that perfect gluing bifurcation cannot be observed in real experiment, since the symmetry is impaired due to several sources of imperfections as well as the presence of noise inherent in any experiment. However, we observed pairs of period-2 limit cycles $(0^2, 1^2)$, period-1 (0 and 1) limit cycles and a pair of big period-1 limit cycles $(10, 01)$ as shown in Fig. 9 by changing either R_1 or R_p values. Moreover, we observed, in experiment, a limit cycle labeled by 100 for an intermediate R_1 value as described below in two different experiments. Similar to numerical simulations, in experiment too we restrict the dynamics of the circuit to periodic modes only by limiting R_p to an appropriate range.

In a first experiment, R_p is kept fixed at $33.4\,\mathrm{k}\Omega$ and R_1 is decreased from $1430\,\Omega$ to $1310\,\Omega$ and we observe coexisting period-2 limit cycles (0^2 and 1^2) via super-Hopf bifurcation as shown in Fig. 9. However, in contrast to the numerical simulations, the time period plots of 0^2 and 1^2 limit cycles are now distinct and separate as shown in Fig. 10. The periodic orbits now tend to the saddle focus for different values of R_1. It is clearly seen from the period of 0^2 (black trace) and 1^2 (red trace)

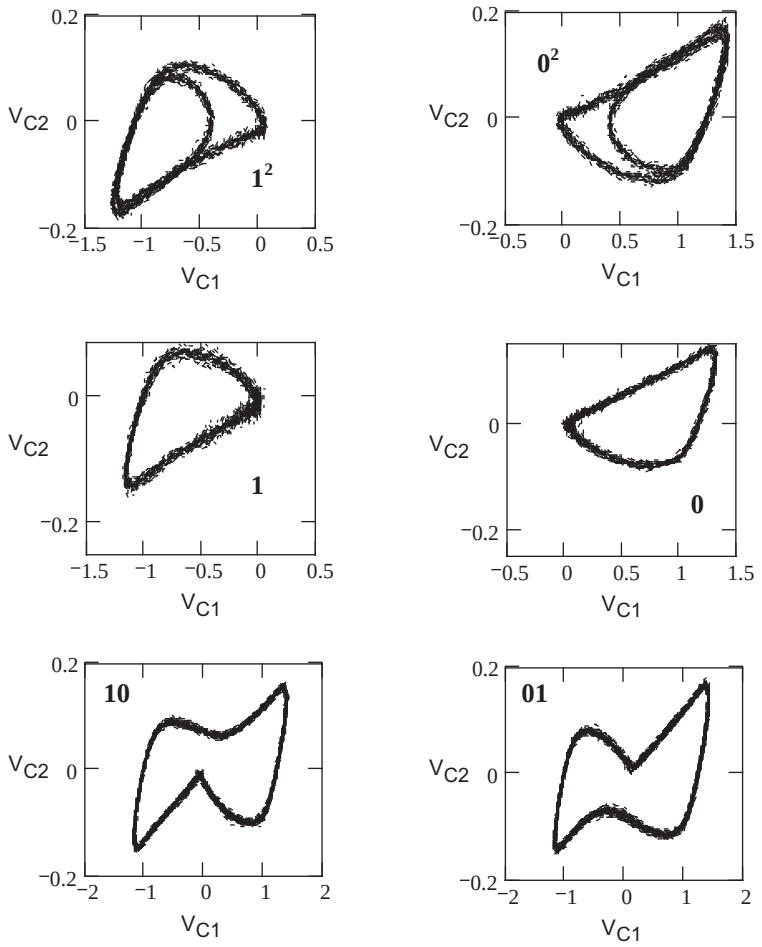

Fig. 9. Experimental gluing bifurcation: coexisting orbits $(1^2, 0^2)$ in the upper row, $(1, 0)$ in middle row and $(10, 01)$ in the lower row ($R_p = 33.4\,\mathrm{k}\Omega$).

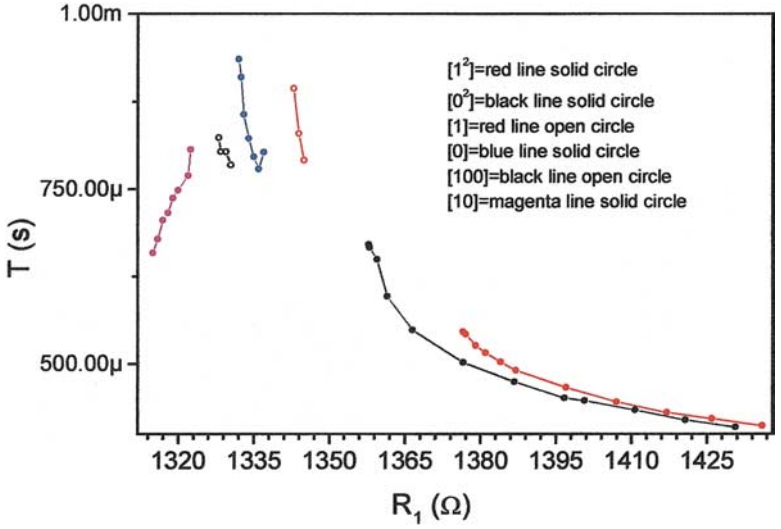

Fig. 10. Experimental period-parameter bifurcation ($R_p = 33.4\,\mathrm{k}\Omega$).

limit cycles that they both increase asymptotically and become homoclinic but for different values of R_1. It is to be noted that 1^2 orbit coexists with 0^2 orbit for a range of R_1 from $1425\,\Omega$ to $1365\,\Omega$ below which 0^2 orbit only exists. The phase portraits and time series of 0^2 and 1 are shown in Figs. 11(a) and 11(c), respectively. Beyond this point ($R_1 < 1365\,\Omega$) on the left side of the period-parameter plot, the curve is disconnected and we find gluing of one stable period-2 orbit and one unstable period-2 orbit via SN bifurcation at $R_1 = 1348\,\Omega$. The corresponding time series and phase portraits of the gluing orbit are shown in Fig. 11(b). The period-parameter (Fig. 10) shows two separate lines on the left for period-1 orbits labeled by 1 (red line) and 0 (black line). They show asymptotic increase in period indicating homoclinicty at $R_1 = 1336\,\Omega$ and $1327.5\,\Omega$, respectively. In the disconnected region between period plots of 1 and 0 orbits we find another gluing of a stable 0^2 orbit and an irregular orbit via SN bifurcation in Fig. 11(d). The corresponding time series and phase portraits of the $(0, 1)$ periodic orbits in Figs. 11(c) and 11(e) and the irregular orbit are shown in Figs. 11(b) and 11(d). The irregular orbit then breaks into a 100 orbit for $R_1 = 1327.4\,\Omega$, whose period (black trace in Fig. 10) again increases asymptotically. The 100 orbit and its time series are shown in Fig. 11(f). Finally, the 100 orbit switch over to a large orbit labeled by 10 (magenta line in Fig. 10) at $R_1 = 1327.2\,\Omega$ after another irregular region. A typical orbit in this irregular region is shown in Fig. 11(g) while 10 orbit is shown in Fig. 9. In Fig. 10 we have specified the periodic regions by continuous lines which are disconnected in irregular regions. These irregular regions are manifested as alternate appearance

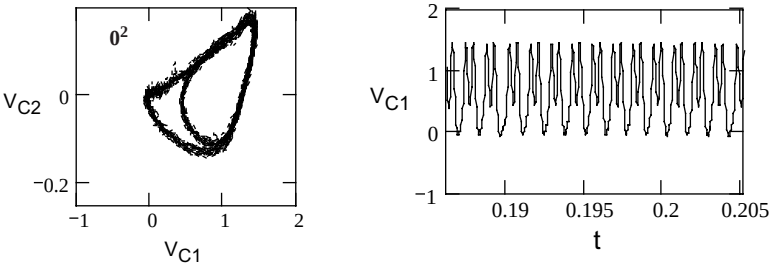

(a)

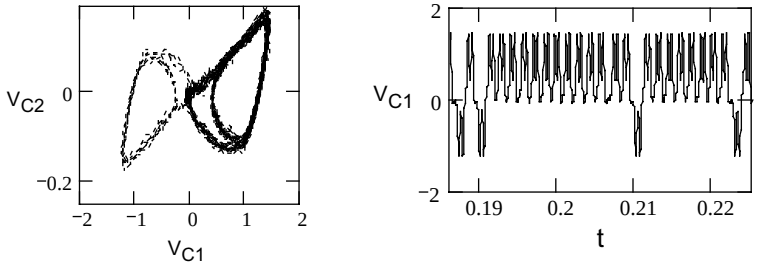

(b)

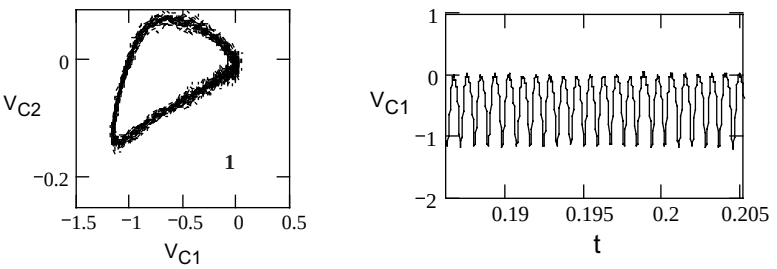

(c)

Fig. 11. Experimental gluing bifurcation: phase portraits and time series ($R_p = 33.4\,\mathrm{k}\Omega$).

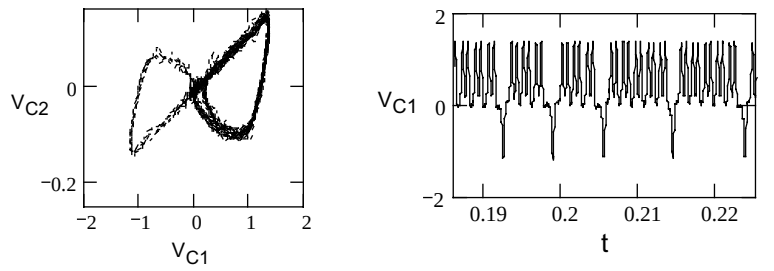

(d)

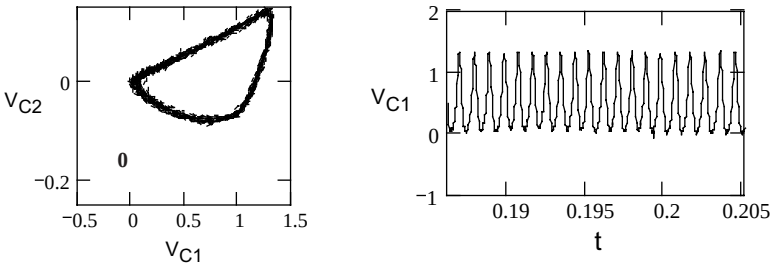

(e)

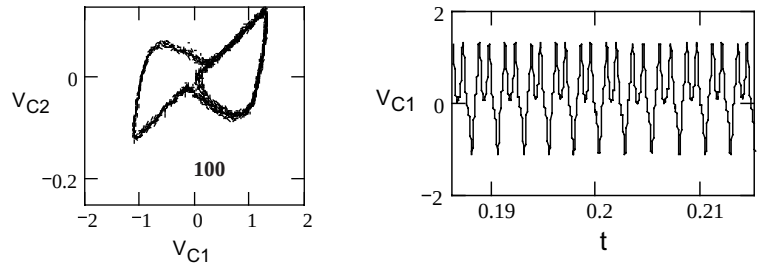

(f)

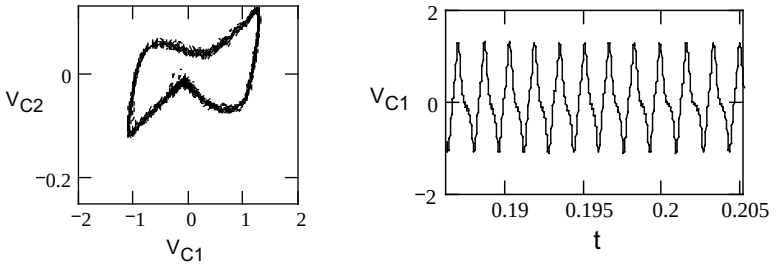

(g)

Fig. 11. (*Continued*)

of irregular and periodic orbits in temporal dynamics.

In a second experiment, we fix $R_1 = 1316\,\Omega$ and increase R_p from $25\,\mathrm{k}\Omega$ when we observe two pairs of asymmetric periodic orbits labeled by (1, 0) and (10, 01). The corresponding phase portraits are shown in Fig. 12. Each periodic orbit is interspersed by alternate irregular orbits in parameter space. The pair of periodic orbits $(0, 1)$ coexists for a range of R_p in period-parameter space (Fig. 13). With increase of R_p the 0 (solid blue circle) and 1 (solid red circle) periodic orbits approach to saddle focus at the origin for different values of $R_p = 28.89\,\mathrm{k}\Omega$ and $R_p = 25.7\,\mathrm{k}\Omega$ respectively. Similar

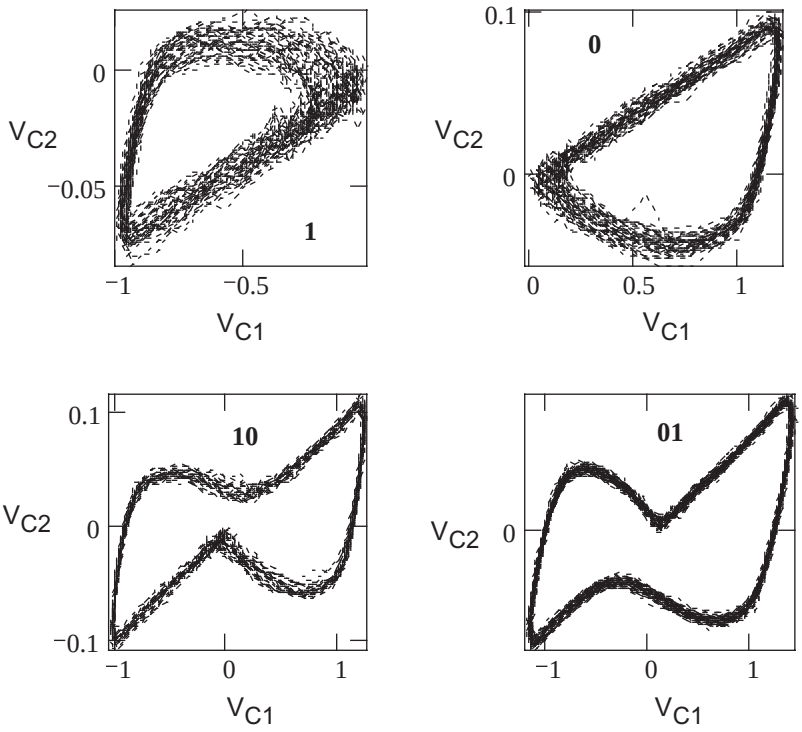

Fig. 12. Experimental phase portraits ($R_1 = 1316\,\Omega$).

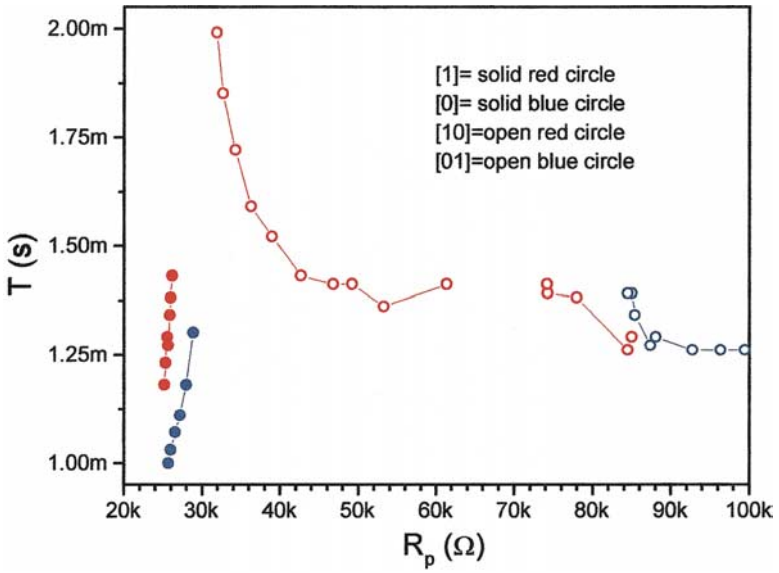

Fig. 13. Experimental period-parameter bifurcation ($R_1 = 1316\,\Omega$).

bifurcation scenario is reported in other systems [Glendenning *et al.*, 2001] too. For $R_p > 28.89\,\mathrm{k}\Omega$, the curve is almost vertical at $R_p = 31.9\,\mathrm{k}\Omega$ when the 0 orbit jumps over to 10 orbit (open red circle) with an intermediate disconnected region of irregular dynamics. This region indicates the existence of intermediate irregular cycles, when a stable 0 and an unstable 1 orbit are being glued to the saddle focus by saddle-node (SN) bifurcation. The curve for 10 periodic orbit continues to decrease monotonically for $R_p > 31.9\,\mathrm{k}\Omega$ before showing an increasing trend again for larger R_p. The period-parameter plot encounter another discontinuity at $R_p = 61.4\,\mathrm{k}\Omega$ until the 10 orbit reappears for $R_p > 74.2\,\mathrm{k}\Omega$ (open red circle dots), whose period goes down hill near $R_p = 84.5\,\mathrm{k}\Omega$. Here we find the

coexisting orbit labeled by 01 (blue open circle) for $R_p = 84.5\,\mathrm{k}\Omega$, which is a mirror image of 10 orbit as shown in Fig. 12. The period of 01 orbit shows a decreasing trend with R_p.

5. Conclusion

We reported our numerical as well as experimental observations on gluing bifurcation in Chua Oscillator. For this we made a simple modification in the original circuit by adding a variable resistance parallel to the nonlinear resistance. This modification limits the dynamics of the oscillator to period-2 orbit only and helps explore the simpler cases of gluing bifurcations. The bistability property and reflection symmetry of the original Chua circuit remain intact with such modification. The bistability is an important criterion for observation of gluing bifurcation phenomena since two mirror symmetric limit cycles can only coexist then.

In gluing bifurcation of Chua model, a pair of symmetric orbits is homoclinic to the saddle focus at the origin for a critical value of the control parameter, when they appear as mirror images of each other. Our observation showed that only one gluing point appears below some critical value of the control parameter R_p, when a pair of $(1, 0)$ orbits merge together. As the value of the control parameter R_p is increased, complication starts growing with the appearance of more gluing points of periodic orbits $(1^2, 0^2)$ and $(1, 0)$. Gluing of higher periodicity orbits at larger R_p value leads to the origin of double scroll chaos in Chua circuit. We restricted our numerical studies to a range of R_p between $10.375\,\mathrm{k}\Omega$ to $11\,\mathrm{k}\Omega$ which gives a fair idea of gluing bifurcation in the dynamics of Chua oscillator.

In experiment, we never found merging of two homoclinic orbits at a single value of the control parameter due to asymmetry in experimental systems induced by noise and other natural imperfections. Instead, we observed homoclinic orbits 1 and 0 for different values of the control parameter R_1 for fixed values of R_p. However, at the edge of transition from stable limit cycle to instability we observed gluing of a stable and a saddle cycle via SN bifurcation. We find alternate sequence of periodic and chaotic states as indicated by continuous lines interspersed by discontinuity in period-parameter space respectively.

Acknowledgments

The work is partially funded by the BRNS, Department of Atomic Energy, Government of India under project Grant No. 2000/34/13-BRNS. P. K. Roy acknowledges partial support by UGC, Government of India, under the Grant No. PSW-040/04-05.

References

Absaghen, J., Pfisher, G. & Mullin, T. [2001] "Gluing bifurcations in a dynamically complicated extended flow," *Phys. Rev. Lett.* **87**, 224501–224504.

Chua, L. O., Komuro, M. & Matsumoto, T. [1986] "The double scroll family — Part I: Rigorous proof of chaos," *IEEE Trans. Cir. Systs.* **CAS-33**, 1072–1097.

Dana, S. K. & Chakraborty, S. [2004] "Generation of homoclinic oscillation in the phase synchronization regime in coupled Chua's oscillators," *Int. J. Bifurcation and Chaos* **14**, 1375–1383.

Gaspard, P., Kapral, R. & Nicolis, G. [1984] "Bifurcation phenomena near homoclinic systems: A two parameter analysis," *J. Stat. Phys.* **35**, 697–727.

Glendinning, P. & Sparrow, C. [1984] "Local and global behavior near homoclinic orbits," *J. Stat. Phys.* **35**, 645–696.

Glendinning, P., Absaghen, J. & Mullin, T. [2001] "Imperfect gluing bifurcation," *Phys. Rev. E* **64**, 036208–036215.

Healy, J. J., Broomhead, D. S., Cliffe, K. A., Jones, R. & Mullin, T. [1991] "The origin of chaos in a modified van der Pol oscillator," *Physica D* **48**, 322–339.

Herrero, R., Farjas, J., Pons, R., Pi, F. & Orriols, G. [1998] "Gluing bifurcations in optothermal nonlinear devices," *Phys. Rev. E* **57**, 5366–5377.

Kennedy, M. P. [1993] "Three steps to chaos — Part II: A Chua's circuit primer," *IEEE Trans. Cir. Systs.* **CAS-40**, 640–656.

Marques, F., Lopez, J. M. & Irano, V. [2002] "Imperfect gluing bifurcation in a temporal glide-symmetric Taylor–Couette flow," *Phys. Fluids* **14**, L33–L36.

Paźo, D. & Pérez-Muñuzuri, V. [2002] "Travelling fronts in an array of coupled symmetric bistable units," arXiv.nlin.PS/0205005 v1.

Peacock, T. & Mullin, T. [2001] "Homoclinic bifurcation in a liquid crystal flow," *J. Fluid. Mech.* **432**, 369–386.

Silva, C. P. [1993] "Shil'nikov's theorem — a tutorial," *IEEE Trans.* **CAS-I 40**, 675–682.

Wiggins, S. [1990] *Introduction to Applied Nonlinear Dynamical Systems and Chaos* (Springer-Verlag, NY).

Zebrwoski, J. J. & Baranowski, R. [2003] "Direct observation of homoclinic orbits in human heart rate variability," *Phys. Rev. E* **67**, 056216–6.